LBL-23463 c.2

Lawrence Berkeley Laboratory
UNIVERSITY OF CALIFORNIA

APPLIED SCIENCE DIVISION

RECEIVED
LAWRENCE
BERKELEY LABORATORY

JUN 26 1987

LIBRARY AND
DOCUMENTS SECTION

Presented at the Twenty-First Symposium (International)
on Combustion, Munich, W. Germany, August 3–8, 1986

FLAME INDUCED VORTICITY: EFFECTS OF STRETCH

M.-Z. Pindera and L. Talbot

August 1986

TWO-WEEK LOAN COPY

This is a Library Circulating Copy
which may be borrowed for two weeks.

APPLIED SCIENCE DIVISION

LBL-23463 c.2

Prepared for the U.S. Department of Energy under Contract DE-AC03-76SF00098

DISCLAIMER

This document was prepared as an account of work sponsored by the United States Government. While this document is believed to contain correct information, neither the United States Government nor any agency thereof, nor the Regents of the University of California, nor any of their employees, makes any warranty, express or implied, or assumes any legal responsibility for the accuracy, completeness, or usefulness of any information, apparatus, product, or process disclosed, or represents that its use would not infringe privately owned rights. Reference herein to any specific commercial product, process, or service by its trade name, trademark, manufacturer, or otherwise, does not necessarily constitute or imply its endorsement, recommendation, or favoring by the United States Government or any agency thereof, or the Regents of the University of California. The views and opinions of authors expressed herein do not necessarily state or reflect those of the United States Government or any agency thereof or the Regents of the University of California.

To Appear In The

Twenty-First Symposium (International) on Combustion

Munich, August 3-8, 1986

FLAME INDUCED VORTICITY: EFFECTS OF STRETCH

by

M.-Z. Pindera and L. Talbot

UNIVERSITY OF CALIFORNIA
Department of Mechanical Engineering
Applied Science Division
Lawrence Berkeley Laboratory
University of California
Berkeley, California 94720

Keywords:

(10) Flames
(11) Fluid Dynamics
(18) Modeling and Scaling

ABSTRACT

In many combustion situations, the flame may be regarded as an interface separating fluids of different densities: fresh reactants from burnt products. Basic considerations of such thin flames indicate that in general the velocity field in the burnt regions is rotational; that is, flames produce vorticity. The circulation of the above flow depends linearly on the flame stretch. In order to account for the jump in normal velocity across the flamefront, the flame may be thought to consist of a collection of sources whose strength depends on the density ratio and the laminar flame speed. For flames of finite length it is shown that the cumulative action of these sources induces an additional contribution to the stretch, and thus to the circulation. The sense of rotation of this flame-induced circulation is such as to decrease the flame-induced stretch. The effects of vorticity production on the velocity field is illustrated for the case of the stretch caused by the presence of the flame only, and for the stretch dominated by cold flow inhomogeneities, in steady flow conditions. The results indicate that for flames of finite extent, the production of vorticity forms an integral part of the overall velocity field and that ignoring the effects of fluid rotation may lead to results not in accordance with experiment.

1. INTRODUCTION

In recent years a considerable amount of research has been expended on numerical studies of dynamics of flames and their influence on the surrounding flow field. For premixed reactants, a fruitful approach has been found by treating the flame as a "slightly compressible" interface separating otherwise dynamically incompressible fresh reactants from burnt products. In the context used, "slightly compressible" means that the effects of flame exothermicity are manifested only through volumetric expansion which is confined to a very narrow (in principle infinitesimally thin) flame region. The flame is thus taken as a collection of sources embedded in a flow of uniform density and pressure. The implied assumption here is that since the combustion process occurs at low Mach numbers, it is permissible to take the pressure field to be spatially uniform throughout. Works of Ghoniem et al.[1], Sethian[2] and Ashurst[3] provide examples of such an approach.

The aim of this paper is to examine some of the theoretical difficulties associated with such methods, and to provide a possible resolution of these problems. Below we outline the general principles involved. As with the methods cited above, the analysis is for strictly two-dimensional flow.

Essentially, the models are based on the fact that in most situations, a general vector field $\underset{\sim}{U}$ (in this case velocity) may be decomposed into three linearly additive components[4]*,

$$\underset{\sim}{U} = \underset{\sim}{U}_c + \underset{\sim}{U}_v + \underset{\sim}{V} \tag{1.1}$$

Define

$$\underset{\sim}{\nabla} \cdot \underset{\sim}{U} = \mathcal{E}(\underset{\sim}{x})$$

$$\underset{\sim}{\nabla} \times \underset{\sim}{U} = \underset{\sim}{\omega}(\underset{\sim}{x})$$

where $\mathcal{E}(\underset{\sim}{x})$ and $\omega(\underset{\sim}{x})$ represent the compressibility effects and the vorticity field, respectively.

---

*The symbols are defined at the end of the paper.

1. INTRODUCTION

In recent years a considerable amount of research has been expended on numerical studies of dynamics of flames and their influence on the surrounding flow field. For premixed reactants, a fruitful approach has been found by treating the flame as a "slightly compressible" interface separating otherwise dynamically incompressible fresh reactants from burnt products. In the context used, "slightly compressible" means that the effects of flame exothermicity are manifested only through volumetric expansion which is confined to a very narrow (in principle infinitesimally thin) flame region. The flame is thus taken as a collection of sources embedded in a flow of uniform density and pressure. The implied assumption here is that since the combustion process occurs at low Mach numbers, it is permissible to take the pressure field to be spatially uniform throughout. Works of Ghoniem et al.[1], Sethian[2] and Ashurst[3] provide examples of such an approach.

The aim of this paper is to examine some of the theoretical difficulties associated with such methods, and to provide a possible resolution of these problems. Below we outline the general principles involved. As with the methods cited above, the analysis is for strictly two-dimensional flow.

Essentially, the models are based on the fact that in most situations, a general vector field $\underset{\sim}{U}$ (in this case velocity) may be decomposed into three linearly additive components[4]*,

$$\underset{\sim}{U} = \underset{\sim}{U}_{\varepsilon} + \underset{\sim}{U}_{\omega} + \underset{\sim}{V} \tag{1.1}$$

Define

$$\underset{\sim}{\nabla} \cdot \underset{\sim}{U} = \varepsilon(\underset{\sim}{x})$$

$$\underset{\sim}{\nabla} \times \underset{\sim}{U} = \underset{\sim}{\omega}(\underset{\sim}{x})$$

where $\varepsilon(\underset{\sim}{x})$ and $\omega(\underset{\sim}{x})$ represent the compressibility effects and the vorticity field, respectively.

---

*The symbols are defined at the end of the paper.

Then

$$\underset{\sim}{\nabla}\cdot\underset{\sim}{U}_e = \epsilon(\underset{\sim}{x}) \quad , \underset{\sim}{\nabla}\times\underset{\sim}{U}_e = 0 \quad ; \underset{\sim}{U}_e \text{ is irrotational} \tag{1.2}$$

$$\underset{\sim}{\nabla}\cdot\underset{\sim}{U}_v = 0 \quad , \quad \underset{\sim}{\nabla}\times\underset{\sim}{U}_v = \underset{\sim}{\omega}(\underset{\sim}{x}) \; ; \; \underset{\sim}{U}_v \text{ is solenoidal} \tag{1.3}$$

(1.4)

Equations (1.2), (1.3) may be cast into Poisson-type forms, which in turn may be solved using Green's functions to give

$$\underset{\sim}{U}_e = \frac{1}{2\pi}\int_A \frac{\epsilon(\underset{\sim}{x}')\underset{\sim}{r}\, dA(\underset{\sim}{x}')}{r^2} \quad ; \quad \underset{\sim}{r} = \underset{\sim}{x} - \underset{\sim}{x}' \tag{1.5}$$

$$\underset{\sim}{U}_v = \frac{1}{2\pi}\int_A \frac{\underset{\sim}{r}\times\underset{\sim}{\omega}(\underset{\sim}{x}')\, dA(\underset{\sim}{x}')}{r^2} = \frac{1}{2\pi}\int_A \frac{\omega(\underset{\sim}{x}')}{r^2}\left[(x-x')\underset{\sim}{j} - (y-y')\underset{\sim}{i}\right] dA(\underset{\sim}{x}') \tag{1.6}$$

while the velocity $\underset{\sim}{V}$ is obtained from a solution to the Laplace's equation

$$\nabla^2\varphi = 0 \quad ; \quad \underset{\sim}{V} = \underset{\sim}{\nabla}\varphi \tag{1.7}$$

subject to appropriate boundary conditions.

The above equations indicate how, in principle, the velocity field may be found given the distribution of $\epsilon(\underset{\sim}{x})$ and $\omega(\underset{\sim}{x})$. The problem is then reduced to one of tracking the vorticity field $\omega(\underset{\sim}{x})$, and of tracking the flamefront represented by $\epsilon(\underset{\sim}{x})$. The former is treated using the method of discrete vortex dynamics developed by Chorin[5]. The effects of the flame front are discussed in the next section.

2. FLAME MODEL

As stated previously, the flame acts as an interface between fresh and burnt gases. The velocity field due to volumetric expansion effects is accounted for - according to the velocity decomposition Eq. (1.1) - by Eq. (1.5).

For simplicity, suppose the flame is composed of a number of straight line

segments. For an interface, Eq. (1.5) is evaluated by letting the interface thickness shrink to zero in such a way that

$$\lim_{\text{thickness}\to 0}(\varepsilon(\underset{\sim}{x})\cdot\text{thickness}) = \text{constant};\ \bar{m}\ \text{say, strength per unit length}$$

For a segment of length L, Eq. (1.5) becomes

$$\underset{\sim}{U}_e = \frac{1}{2\pi}\int_0^L \frac{\bar{m}(\underset{\sim}{x}')\underset{\sim}{r}\,dx'}{r^2} \tag{2.1}$$

If the source strength m is constant, the velocity components at any point (x_0, y_0), with respect to the local flame coordinates (tangential and normal), become[6]

$$U_t(x_0,y_0) = \frac{(\nu-1)S_u}{2\pi}\ln\left(\frac{r_1}{r_2}\right) \tag{2.2}$$

$$U_n(x_0,y_0) = \frac{(\nu-1)S_u}{2\pi}(\theta_2-\theta_1) \tag{2.3}$$

where one may show that $m=(\nu-1)S_u$ (see[1], for example). The parameters r_1, r_1, θ_1 and θ_2 are explained in Fig. 1 below.

At the flamefront $(\theta_1=0, \theta_2=\pi, r_1+r_2=L)$ the normal velocity is uniform as expected and as indicated by Eq. (2.3). The tangential velocity however is anti-symmetrical about the centerline $r_1=r_2$, increasing towards the ends of the flame segment (this is also felt throughout the whole field) and becomes logarithmically singular at the ends themselves. Such a velocity field is characteristic of a source representation, since the sources tend to act cumulatively.

The singular behavior is not a very serious deficiency of the model since it should be possible to remove it by defining a suitable source strength distribution $m(\underset{\sim}{x})$, with $m(\underset{\sim}{x})$ decreasing faster than the growth of the singularity. Doing this may be justified for mixtures where the Lewis number is greater than unity, and preferential diffusion is of importance, as discussed

by Wu[7], whose experimental data indicates that for Le > 1, the flame temperature (and hence ν) should decrease with the increase of "pure" flame stretch K. Here, pure stretch refers to stretch induced by flow nonuniformities and corresponds to the first contribution to the total stretch defined below

$$K = \frac{1}{A}\frac{dA}{dt} = \underset{\sim}{\nabla}_t \cdot \underset{\sim}{U}_t - \frac{\underset{\sim}{U}_t \cdot \underset{\sim}{n}}{R} \tag{2.4}$$

According to Eq. (2.2) evaluated at the flamefront, with

$$K_{pure} = \underset{\sim}{\nabla}_t \cdot \underset{\sim}{U}_t = \frac{\partial U_t}{\partial t} = \frac{(\nu-1)L S_u}{2\pi t(L-t)} \tag{2.5}$$

Hence the flame induced stretch is positive and singular at the segment ends ($t=0, t=L$) and may be used within the framework of the present model to decrease the source strength (for Le > 1) to conform to the current theories and observations.

A more serious difficulty is caused by the fact that the induced tangential velocity will tend to create large pressure gradients along the flamefront. As shown in the next section, this suggests that the effect of baroclinic production of vorticity at the flamefront may not be negligible.

3. VORTICITY PRODUCTION

Production of vorticity at the interface dividing two media of different densities have been studied by various people[8,9,10], and the algebraic relations for the magnitude of the resultant vorticity are known. Below we present a slightly different approach to highlight the features of the 2-D source flow model. The analysis, as in the studies cited above, applies to inviscid fluid only.

For the case of compressible flow, the rate of change of circulation

in the interior of an ideal fluid is

$$\frac{d\Gamma}{d\tau} = \int_A \left[\frac{1}{\rho^2}\nabla\rho \times \nabla p\right]\cdot \mathbf{b}\, dA \tag{3.1}$$

where $\mathbf{b}$ is the outward unit normal to the area of integration. Define the rate of production of circulation per unit area $\bar{\Gamma}$ to be

$$\frac{d\bar{\Gamma}}{d\tau} = \frac{1}{\rho^2}\left(\nabla\rho \times \nabla p\right)\cdot \mathbf{b} \tag{3.2}$$

For a 2-D flame surface (viewed as a line in the x-y plane) we can label

$$\nabla\rho = \mathbf{n}\nabla_n\rho + \mathbf{t}\nabla_t\rho \tag{3.3}$$

$$\nabla p = \mathbf{n}\nabla_n p + \mathbf{t}\nabla_t p \tag{3.4}$$

with $\mathbf{n}, \mathbf{t}$ being unit vectors in the normal and tangential directions respectively, as shown in Fig. 2 below, such that $(\mathbf{t}, \mathbf{b}, \mathbf{n})$ form a right handed system, that is $\mathbf{b} = \mathbf{t} \times \mathbf{n}$. In light of Eqs. (3.3), (3.4) we observe that the vector $\nabla\rho \times \nabla p$ has no component in the $\mathbf{n}$ direction which implies that the resultant circulation produced by the flow has no component in that direction (i.e. is tangential to the flame). Also, in a two-dimensional flow, since is in the direction normal to (and out of) the page, the fluid has circulation in the plane of the page. Combining Eqs. (3.3), (3.4) into (3.2) and assuming constant density flow on each side of the interface ($\nabla_t\rho = 0$), yields

$$\frac{d\bar{\Gamma}}{d\tau} = -\frac{1}{\rho^2}(\nabla_n\rho)(\nabla_t p) \tag{3.5}$$

We now apply the above equation to a parcel of fluid moving with speed S and crossing a flamefront of vanishingly small thickness Δd in the direction $-\mathbf{n}$. Then approximately

$$d\tau \simeq \frac{\Delta d}{S} \tag{3.6}$$

$$\nabla_n \rho \simeq \frac{\Delta\rho}{-\Delta d} \simeq \frac{\rho_b - \rho_u}{-\Delta d} = \frac{\rho_b(\nu-1)}{\Delta d} \tag{3.7}$$

For steady flow ($\underset{\sim}{U}_t \cdot \underset{\sim}{n} = 0$)

$$\nabla_t p = -\rho\left(U_t \frac{\partial U_t}{\partial t} + U_n \frac{\partial U_n}{\partial n}\right)$$

Since for inviscid flow the tangential velocity does not change across the flamefront, we get

$$\nabla_t p \simeq -\rho U_t \frac{\partial U_t}{\partial t} \tag{3.9}$$

where we have also used the statement of mass conservation across the flamefront,

$$\rho S = \rho_u S_u = \rho_b S_b$$

Equation (3.9) corresponds to the steady state vorticity results of[8,9,10]. Finally, using the steady form of the flame stretch, Eq. (2.5), we get

$$\bar{\Gamma} = \left(\frac{\nu-1}{\nu S_u}\right) U_t K \tag{3.10}$$

From the above equation we observe that since the flame induced stretch is always positive, the resultant circulation in the burnt gases always takes on the sign of the tangential velocity. (In a right-handed system, positive circulation requires counterclockwise fluid motion). The resultant circulation thus tends to counteract the induced velocity gradient and the accompanying singularities in the source induced velocity field. Note however that Eq. (3.10) is valid for any velocity field within the context of our 2-D model. A sketch of the behavior of the flame induced tangential velocity, stretch and

circulation along the flamefront (Eqs. (2.2), (2.5), (3.10)) is shown in Fig. 3 below.

4. NUMERICAL MODEL

The ideas outlined above have been implemented by a numerical algorithm in the following manner. The continuous flame sheet is discretized by a finite number N of elements of length L and total stength m. Each segment in turn is treated as a "blob" of finite radius r_o and total flux m such that

$$m = 2u_f L = 2\pi r_o u_f = (\nu - 1) S_u \pi r_o \tag{4.1}$$

where u_f is the source velocity, Eq. (2.3), evaluated at the flamefront. This type of discretization is consistent with Eq. (2.1) in the limit $N \to \infty$ and $L \to 0$, since then the line source behaves as point source, which can be considered as a primary element of the line source[6].

The velocity field at any point (x_m, y_m) due to the N sources is then

$$\underset{\sim}{u}_e(x_m, y_m) = \frac{1}{2\pi} \sum_{n=1}^{N} \frac{m_n}{r_{nm}^2} \left[(x_m - x_n)\underset{\sim}{i} + (y_m - y_n)\underset{\sim}{j} \right] \tag{4.2}$$

In the above summation, a blob cannot induce velocity or itself, i.e. $m \neq n$. In order to account for consumption of reactants, the flamefront is endowed with a normal propagation velocity S_n in the direction of fresh gases, such that

$$S_n = S_u + u_f \tag{4.3}$$

the last term being added to account for the flame pushing fresh fluid away from itself with velocity . The complete velocity field at the flamefront is then

$$\underset{\sim}{U}_f = S_n \underset{\sim}{n} + U_e + U_v + V \tag{4.4}$$

The flamefront displacement may be calculated by integrating the above equation using a suitable numerical scheme. Thus for a given timestep $\Delta\tau$, a flame point at $\underset{\sim}{X}_f(\tau)$ is moved to a point $\underset{\sim}{X}_f(\tau+\Delta\tau)$ such that

$$\underset{\sim}{X}_f(\tau+\Delta\tau) = \underset{\sim}{X}_f(\tau) + \int \underset{\sim}{U}_f(\tau)\,d\tau \tag{4.5}$$

The stretch of each segment L_i lying between two adjacent flame points $\underset{\sim}{X}_f$ is calculated by directly applying Eq. (2.4),

$$K_i = \frac{1}{L_i(\tau)} \frac{L_i(\tau+\Delta\tau) - L_i(\tau)}{\Delta\tau} \tag{4.6}$$

This value of stretch was used in Eq. (3.10), along with $U_t = \underset{\sim}{U}\cdot\underset{\sim}{t}$ to calculate $\bar{\Gamma}$. In addition, in order to avoid Landau-type instability[11] we allowed the burning velocity S_u to vary with stretch, in accordance with the ideas of Markstein[12] and Clavin and Joulin[13], viz

$$S_u = S_L\left(1 - \frac{\delta K}{S_L}\right) \tag{4.7}$$

where S_L is the plane laminar burning velocity and δ is the Markstein length scale.

Because of the dependence of the flame generated circulation and S_u on the flame stretch, the flame propagation problem is implicit. Hence Eq. (4.5) is solved iteratively using a second order Runge-Kutta scheme. Various trials have shown that the values for the flame position were sufficiently well converged after five iterations.

The strength Γ (circulation) of vorticity at each flame segment was calculated according to

$$\Gamma_i = \bar{\Gamma}_i A_i$$

(4.8)

with A_i being the area swept out by a parcel of burnt fluid during time step $\Delta\tau$, from each flame segment of length L_i, thus

$$A_i = L_i S_{b(i)} \Delta\tau = \nu L_i S_{u(i)} \Delta\tau$$

The resulting vorticity is then treated in a discrete manner, is injected behind each flame segment in the burnt region, and is allowed to be convected and diffused as vortex blobs of finite radius $r_i = \sqrt{A_i/\pi}$, in accordance with the model of Chorin. In order to avoid dealing with an excessive number of vortices - which are injected at every time step and behind every flame element -, the vortices are combined within cells formed by a nonuniform rectangular grid, with the cell size increasing with the increasing distance from the flamefront. This was a compromise between accuracy and computational costs; we have tried to keep a high resolution of the vortex field near the flamefront where the feedback between flame and vorticity production is the greatest, without introducing too many vortices in the flowfield. In each cell vortices were combined so as to preserve the three vorticity invariants

$$\Gamma = \sum_i \Gamma_i$$

$$X = \frac{1}{\Gamma} \sum_i x_i \Gamma_i \quad ; \quad Y = \frac{1}{\Gamma} \sum_i y_i \Gamma_i$$

$$D^2 = \frac{1}{\Gamma} \sum_i \Gamma_i \left[(x_i - X)^2 + (y_i - Y)^2 \right]$$

where Γ, (X,Y) and D are the circulation, position and diameter of the resultant vortex. The grid however was of finite extent and any vortices falling outside of it were removed from the flow.

The combined motion of flame displacement and vortex motion was accomplished using the method of fraction steps (see for example Ghoniem et al.[1]).

Finally, referring to Eq. (4.5), the displaced points were curve fitted using a parametric cubic spline routine and the resulting curve was subdivided into N equally spaced segments. These new points provided a new flame data set and the calculations were repeated as outline above, for the subsequent time step.

5. EXAMPLES AND DISCUSSION

We report some of the results of two test cases we have studied:

a) a stagnation point stabilized flame, and

b) a rod stabilized flame.

Since the first case has strong cold flow inhomogeneities, while in the second the flow inhomogeneities are all due to the presence of the flame, the two cases provide two flow extremes which a stead-state flame may be expected to experience. The results, with and without vorticity are compared to the data of Wu et al.[7] and Cheng[14]. The experimental setups are shown in Fig. 4 and 5. There are some differences between the experiment and the assumptions of the model. For the stagnation point flame, the geometry is axisymmetric and the stagnation plate is finite. In order to duplicate the cold flow stretch we have assumed for our model an axisymmetric ideal cold flow against an infinite plate. The experimental and assumed cold flow profiles are shown in Figs. 6 and 7. The normal velocity profile at the centerline (and hence the centerline cold flow stretch) is well reproduced, however away from the

centerline, the measured profiles show the influence of the finiteness of the stagnation surface. In Fig. 6, the tangential velocity at t = 12.7 mm also shows some boundary layer effects. However, the plots do show similar trends and magnitudes, and the assumed profiles may be taken to be fairly representative of the flow situation. Note that the flame model is for two-dimensional flow only; since however our intent here was to simulate as closely as possible the flame response to cold flow inhomogeneities, the use of a 2-D flame model in an axisymmetric cold flow field is not taken to be a serious deficiency, especially since the two flame models (with and without vorticity) are compared for the same cold flow conditions.

In the second case, the rod stabilized V-shaped flame was in a turbulent flow field and thus in principle it generated an unsteady flow field. Here the flame acted as a "flapping" interface within the wrinkled flame regime. Since the flapping motion appeared to be chaotic, it is not expected that it would add any net contribution to the time averaged velocity fields. In this context, it seems justifiable to use the stationary flame model in comparison of the mean velocities, especially in the region outside of the turbulent flame brush.

The computations were performed taking advantage of the symmetry of the flow fields. In both cases only one half of the flame was modelled; symmetry was exploited using the method of images. The various parameters used in the model are shown in Table 1. The Markstein length was calculated using the model of Clavin and Joulin[13] with Le = 1. In the case of the stagnation point flame, the value was also based on the estimate of the measured flame temperature[15].

Figures 8 and 9 show profiles of the tangential velocity at the indicated stations. As seen from Fig. 8, velocity profile across the flamefront is

misrepresented if no vorticity is included in the calculations. When vorticity is included, the asymptotic values and general trends are representative of those seen in the experiment. As discussed in Ref. 15 the differences that do exist (especially in the central portion of the Figure), may be attributed to the differences in the cold flow profiles and 3-D effects. In particular, the calculated flame position is closer to the burner than the observed, due to the fact that the flame is modelled as an semi-infinite source strip rather than a disc of finite radius. Figure 9 shows the variation of tangential velocity along the flamefront, on the burnt side. In this case, the case of no vorticity shows the proper trend due to the favorable increase of tangential velocity along the flamefront. The computed velocity however is underpredicted rather significantly if the circulation effects are not included.

Figures 10-12 show our results for the time-averaged axial profiles for the V-flame. Figure 10 gives the measured data. Note the existence of velocity defect up to the third measuring station (x = 30 mm) due to the stabilizer induced wake. Note also the large centerline flow acceleration due to streamline divergence. Figures 11 and 12 show computed results without and with the inclusion of vorticity, respectively. In contrast to Fig. 12, or to the experiment, Fig. 11 shows little or no acceleration of fluid in the burnt region. Observed velocities of Fig. 10 do not show the jumps (dotted lines) of Figs. 11 and 12 due to the smearing effect of the turbulent flame brush. The computed velocites of Fig. 12 are generally slightly higher than the measured. This can be attributed to 3-D effects, the semi-infinite flame strip and infinite line vortices as used in our model, will produce higher velocities than those due to a finite flame strip and a finite line vortex, as would be the case in the experiment.

6. CONCLUSION

We have shown that within the source sheet model, the neglect of the source induced pressure gradients may lead to large errors in the computed velocity profiles when compared to the experiment. We may extend the notion of a "slightly compressible" flow however to include vorticity effects; the resultant circulation acts to counter the large gradients produced by the flame alone. The two cases that we have considered have shown that this effect is important regardless whether strong cold flow inhomogenities exist or not, but rather that is is an intrinsic part of the flame model.

Considering the simplicity of our model, our results appear to be encouraging. Work is currently being carried out on the dynamic response of wrinkled flames. Preliminary calculations indicate that the magnitude of the produced circulation may also be represented by Eq. (3.10), where the complete definition for stretch (Eq. 2.4) must now be used.

NOMENCLATURE

A - surface area

Δd - flame thickness

D - diameter of a combined vortex

K - flame stretch

L - length of a flame segment

δ - Markstein length parameter

Le - Lewis Number

m - source strength

P - pressure

r - distance parameter

R - radius of curvature

S - flame speed

S_L - laminar flame speed for a plane flamefront

t - distance parameter along the flamefront

u - flame induced velocity

U - velocity

V - cold flow velocity

X - x-coordinate of the combined vortex

Y - y-coordinate of the combined vortex

ε - source term associted with the flame

Γ - circulation

ν - density ratio $(\nu = \rho_u/\rho_b > 1)$

ω - vorticity

ρ - density

τ - time

θ - angle parameter (see Fig. 1)

SUBSCRIPTS

b - denotes burnt products

a - " irrotational velocity field

f - " variable evaluated at the flamefront

n - " direction normal to the flamefront

t - " " tangential to the flamefront

u - " unburnt reactants

v - " solenoidal velocity field

o - " reference conditions

$\sim$ - (tilde) denotes a vector quantity

SUPERSCRIPTS

$-$ - (dash) denotes a quantity per unit length or per unit area

$'$ - (prime) denotes a dummy variable

UNIT VECTORS

$\underset{\sim}{i}$ - denotes a unit vector along x-axis

$\underset{\sim}{j}$ - " " " " " y-axis

$\underset{\sim}{b}$ - " " " " in the binormal-direction to the flamefront $(\underset{\sim}{b} = \underset{\sim}{t} \times \underset{\sim}{n})$

$\underset{\sim}{n}$ - " " " " " " normal-direction to the flamefront

$\underset{\sim}{t}$ - " " " " " " tangential-direction to the flamefront

ACKNOWLEDGEMENTS

This work was supported by the Director, Office of Energy research, Chemical Sciences Division of the U.S. Department of Energy under Contract DE-AC-03-76SF00098

The authors wish to acknowledge their appreciation to Professor Chorin for the informative comments on the ideas discussed herein. The authors also wish to express their graditude for the patiance, care, and attention given by Ms. Barbara von der Meden to the production of this manuscript.

REFERENCES

1. Ghoniem, A. F., Chorin, A. J. and Oppenheim, A. K., Phil. Trans. R. Soc. A 394, pp. 303-325 (1982).

2. Sethian, J., J. Comp. Phys., 54, pp. 425-465 (1984).

3. Ashurst, W. T. and Barr, P. K., Comb. Sci. and Tech., 34, pp. 227-256 (1983).

4. Batchelor, G. K.: An Introduction to Fluid Dynamics, p. 87, Cambridge University Press (1967).

5. Chorin, A. J., J. Fluid Mech., 57, p. 785 (1973).

6. Pindera, M.-Z., Flame Generated Vorticity, Ph.D. thesis, University of California et Berkeley (1986).

7. Wu, C. K. and Law, C. K., Twentieth Symposium (International) on Combustion, 1941-1949, The Combustion Institute, Pittsburgh (1984).

8. Truesdell, C., J. Aero. Sci., 19, pp. 826-828 (1952).

9. Emmons, H. W. (Ed.), Fundamentals of Gas Dynamics, Vol. III, p. 607, Princeton University Press (1958).

10. Hayes, W. D., J. Fluid Mech., Vol. 2, pp. 595-600 (1959).

11. Landau, L. D. and Lifshitz, E. M., Fluid Mechanics, pp. 478-479, Pergamon Press, 1959.

12. Markstein, G. H. (Ed.), Nonsteady Flame Propagation, pp. 22-24, Macmillan Company (1964).

13. Cheng, R. K., Comb. Sci. and Tech., 25, pp. 127-140 (1984).

14. Clavin, P. and Joulin, G., Le Journal de Physique-Lettres, 44, pp. L-1 - L-12 (1983).

15. Pindera, M.-Z. and Talbot, L., submitted to Physics of Fluids.

LIST OF CAPTIONS

Table 1	Various run parameters
Figure 1	Velocity components due to a 2-D line source
Figure 2	Flamefront geometry
Figure 3	Behavior of K, $\overline{\Gamma}$ and u_t at the flamefront
Figure 4	Stagnation point combustion geometry
Figure 5	Rod anchored flame geometry
Figure 6	Comparison of measured and assumed cold flow tangential velocities
Figure 7	Comparison of measured and assumed cold flow normal velocities
Figure 8	Tangential velocity: measured and calculated with and without vorticity, normal profiles at t = 12.7 mm
Figure 9	Tangential velocity: measured and calculated with and without vorticity, tangential profiles at (H-y) = 4.5 mm
Figure 10	Measured average axial velocities
Figure 11	Calculated axial velocities; no vorticity
Figure 12	Calculated axial velocities; vorticity added

TABLE 1

	S_u (m/s)	ν	$\mathcal{L}$ (m)	Flame elements	Vortices at equilibrium	Timesteps for averaging
Case 1	.14	4	1.6×10^{-4}	80	250	800
Case 2	.44	6.7	10^{-3}	141	270	200

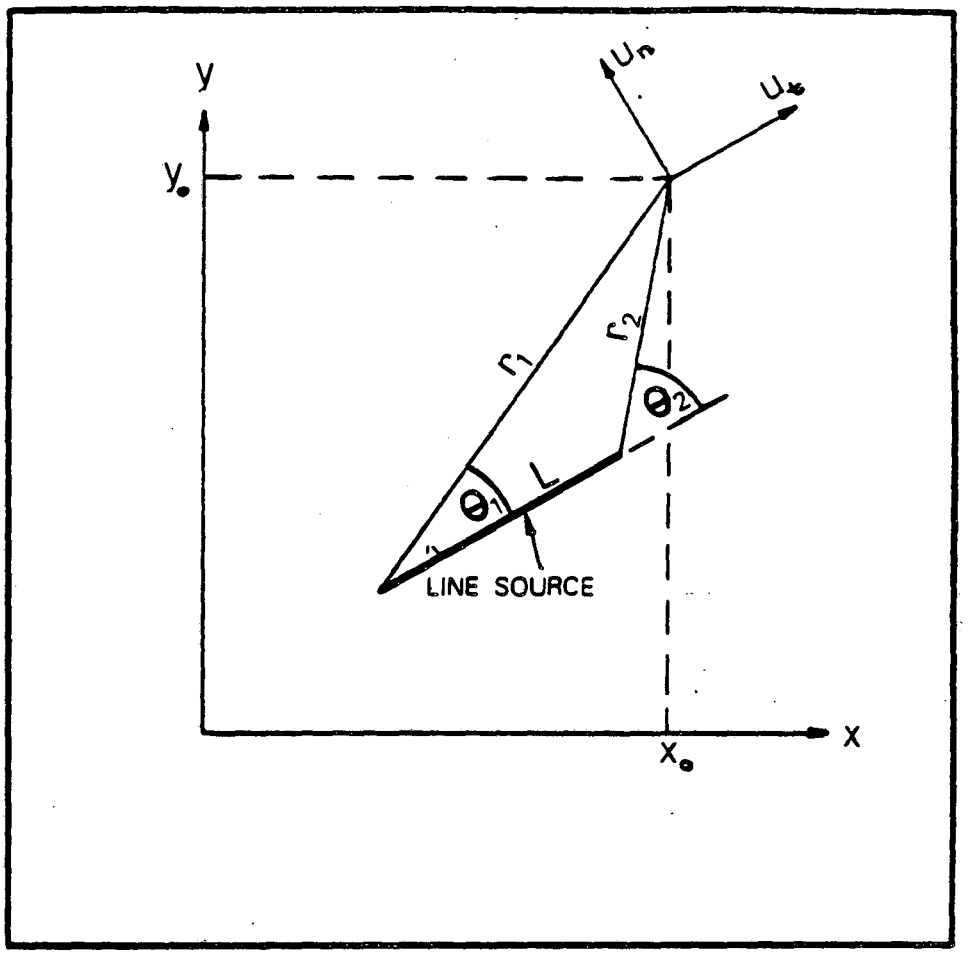

Figure 1

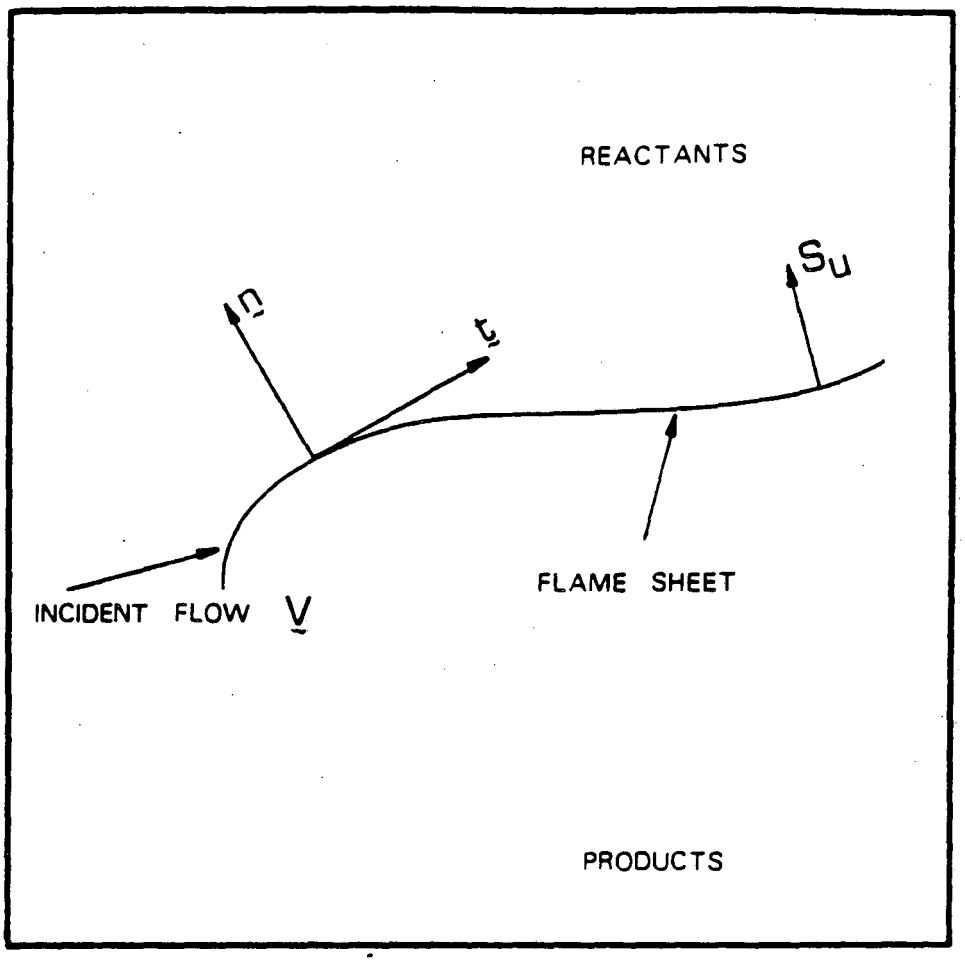
REACTANTS
S_u
$\underset{\sim}{n}$
$\underset{\sim}{t}$
FLAME SHEET
INCIDENT FLOW $\underset{\sim}{V}$
PRODUCTS

Figure 2

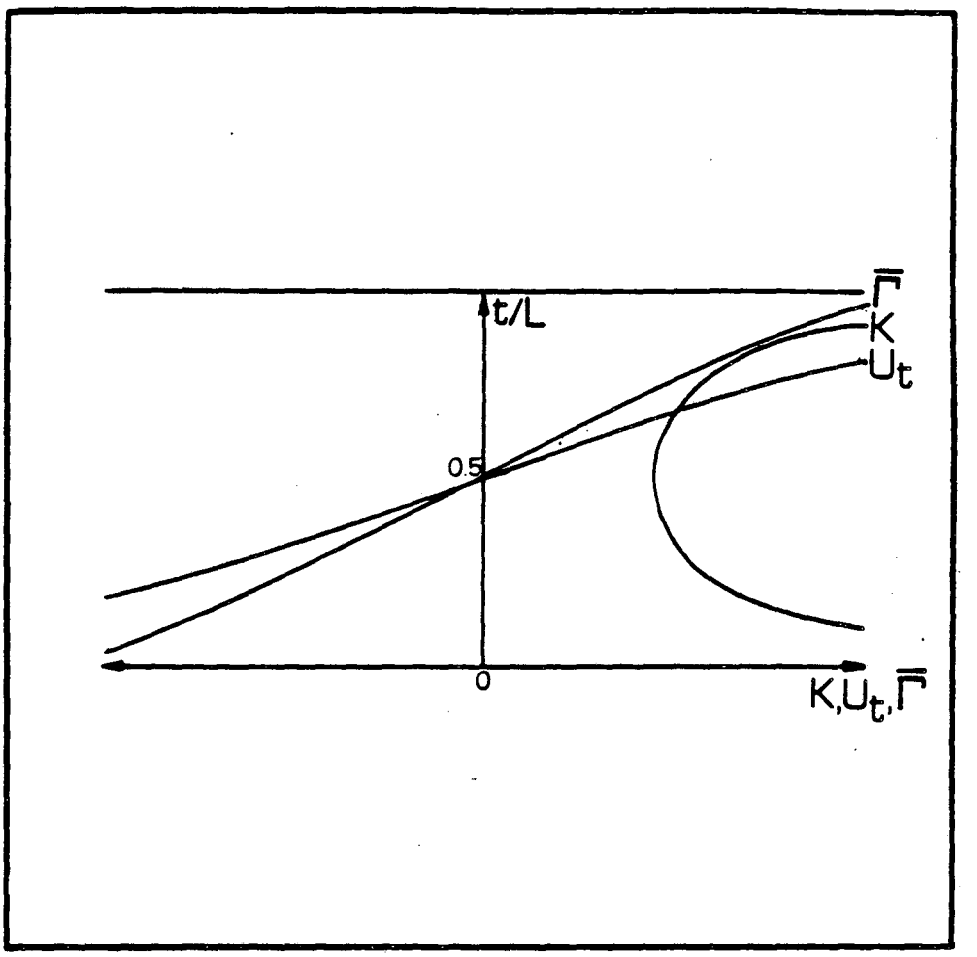

Figure 3

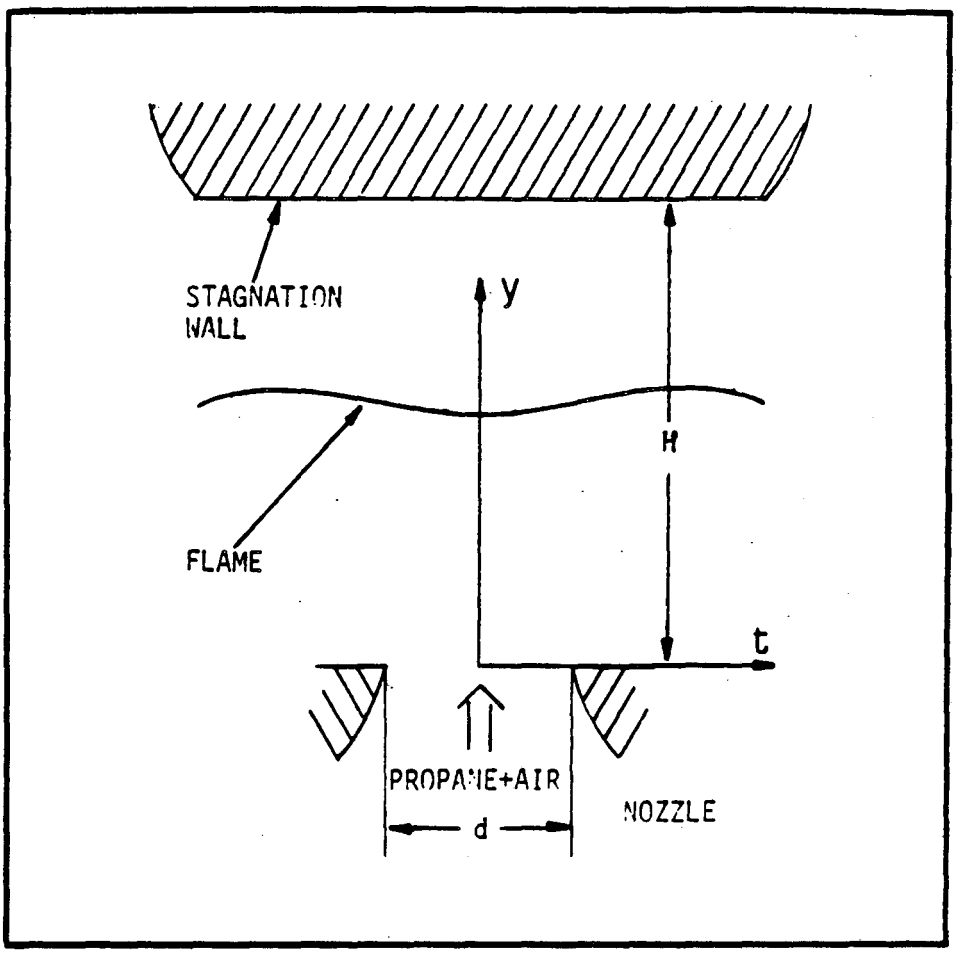

Figure 4

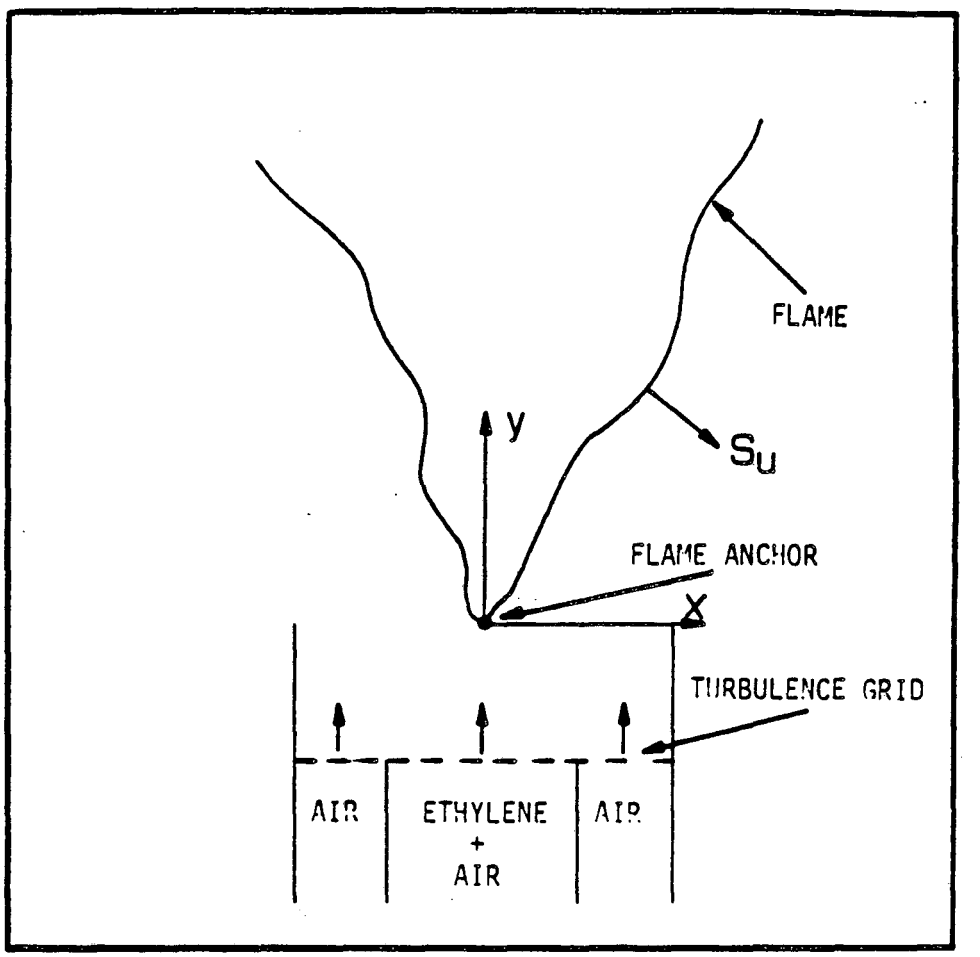
FLAME
y
Su
FLAME ANCHOR
X
TURBULENCE GRID
AIR
ETHYLENE
+
AIR
AIR

Figure 5

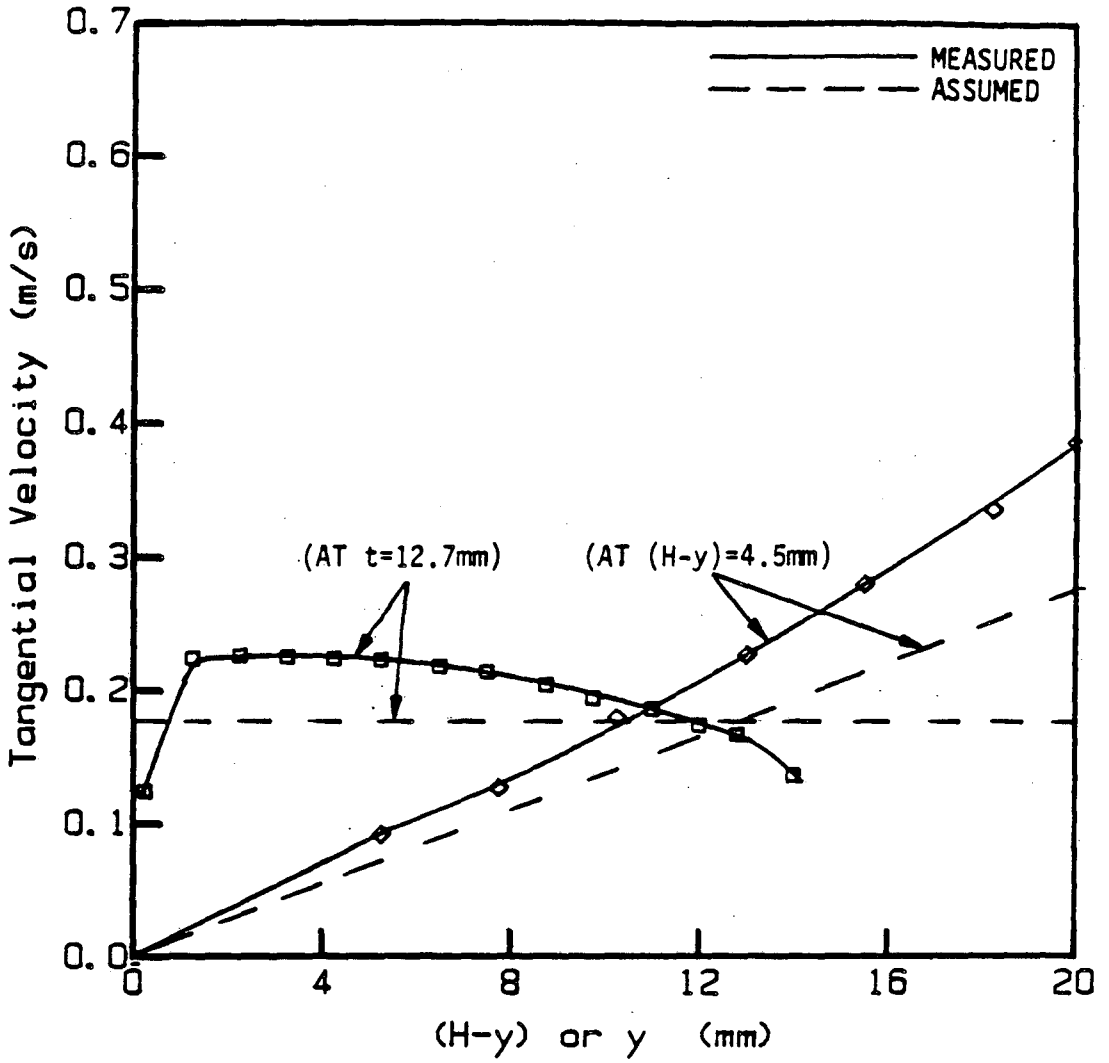
MEASURED
ASSUMED
Tangential Velocity (m/s)
0.7
0.6
0.5
0.4
0.3
0.2
0.1
0.0
(AT t=12.7mm)
(AT (H-y)=4.5mm)
0
4
8
12
16
20
(H-y) or y (mm)

FIgure 6

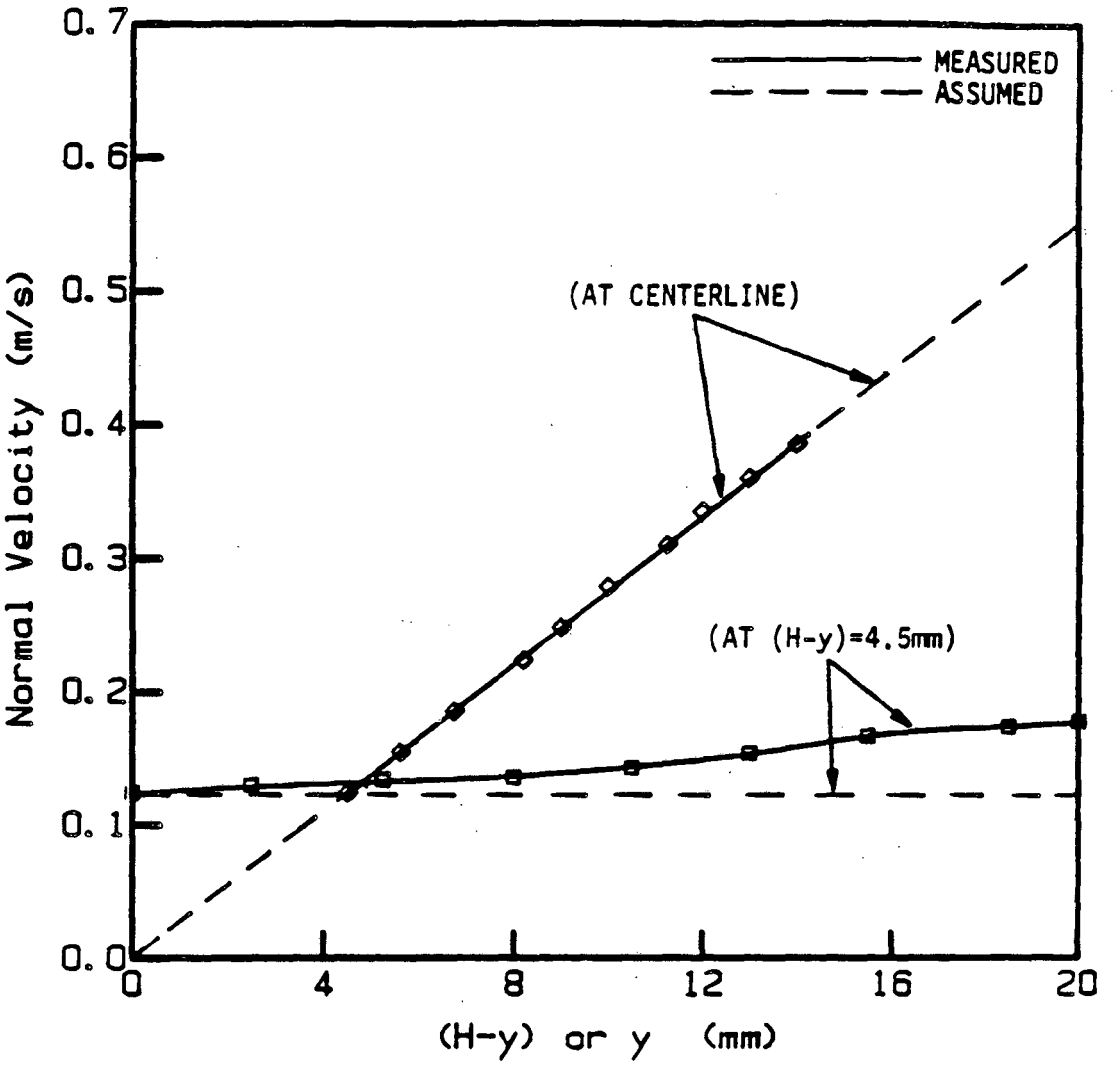
MEASURED
ASSUMED
(AT CENTERLINE)
(AT (H-y)=4.5mm)
Normal Velocity (m/s)
0.0
0.1
0.2
0.3
0.4
0.5
0.6
0.7
0
4
8
12
16
20
(H-y) or y (mm)

FIgure 7

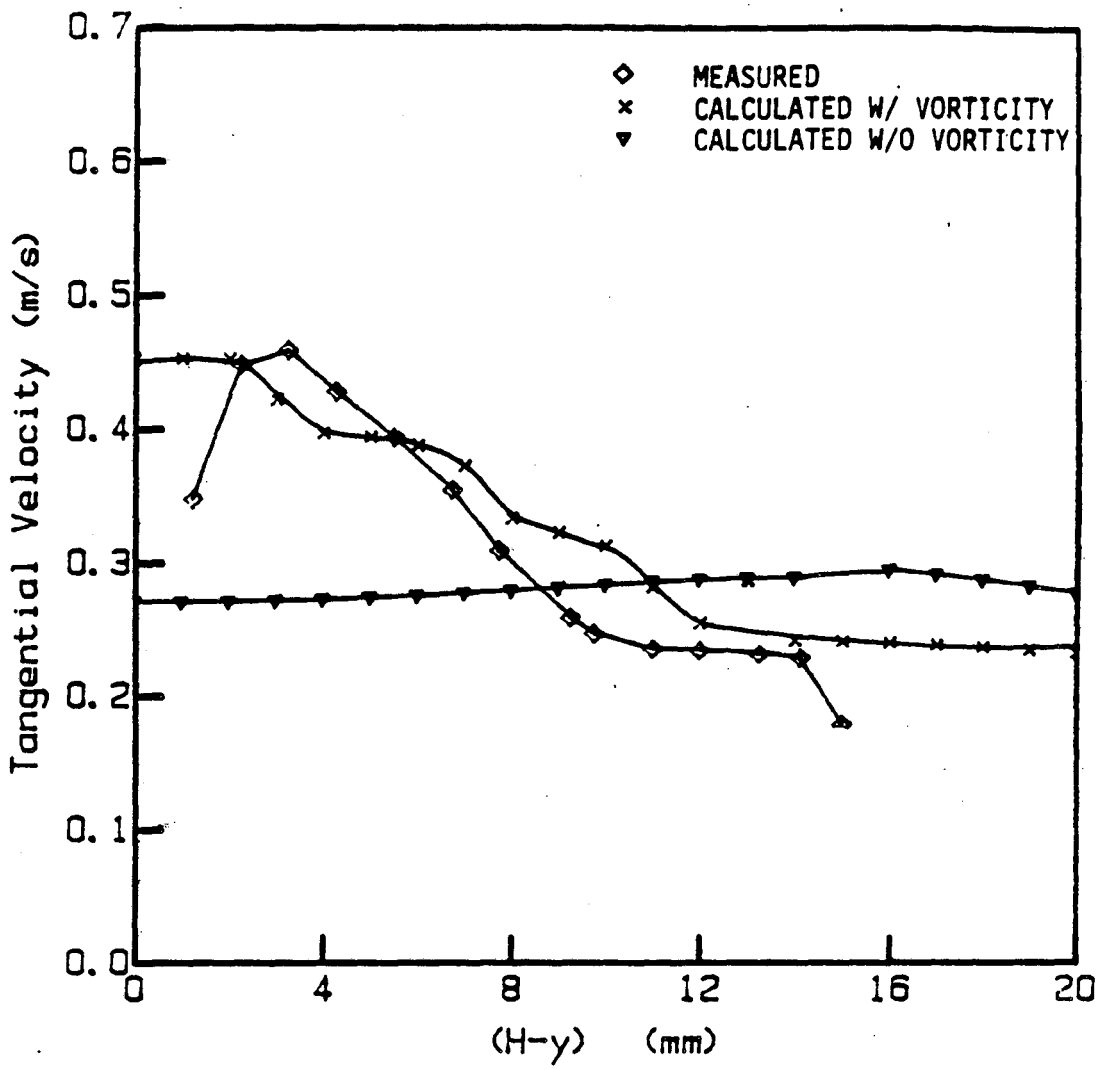
MEASURED
CALCULATED W/ VORTICITY
CALCULATED W/O VORTICITY
Tangential Velocity (m/s)
0.0
0.1
0.2
0.3
0.4
0.5
0.6
0.7
0
4
8
12
16
20
(H-y) (mm)

Figure 8

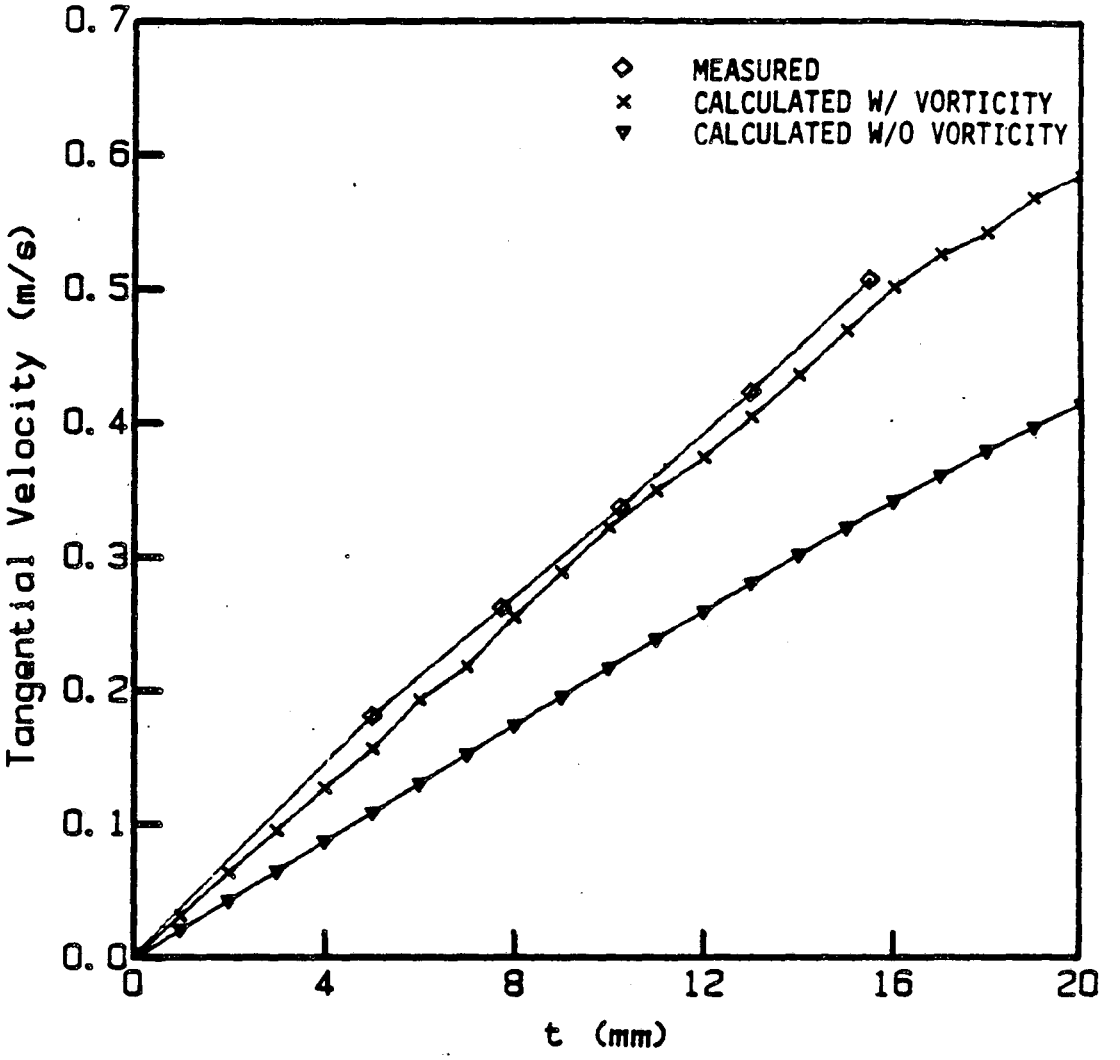
MEASURED
CALCULATED W/ VORTICITY
CALCULATED W/O VORTICITY
Tangential Velocity (m/s)
0.0
0.1
0.2
0.3
0.4
0.5
0.6
0.7
0
4
8
12
16
20
t (mm)

Figure 9

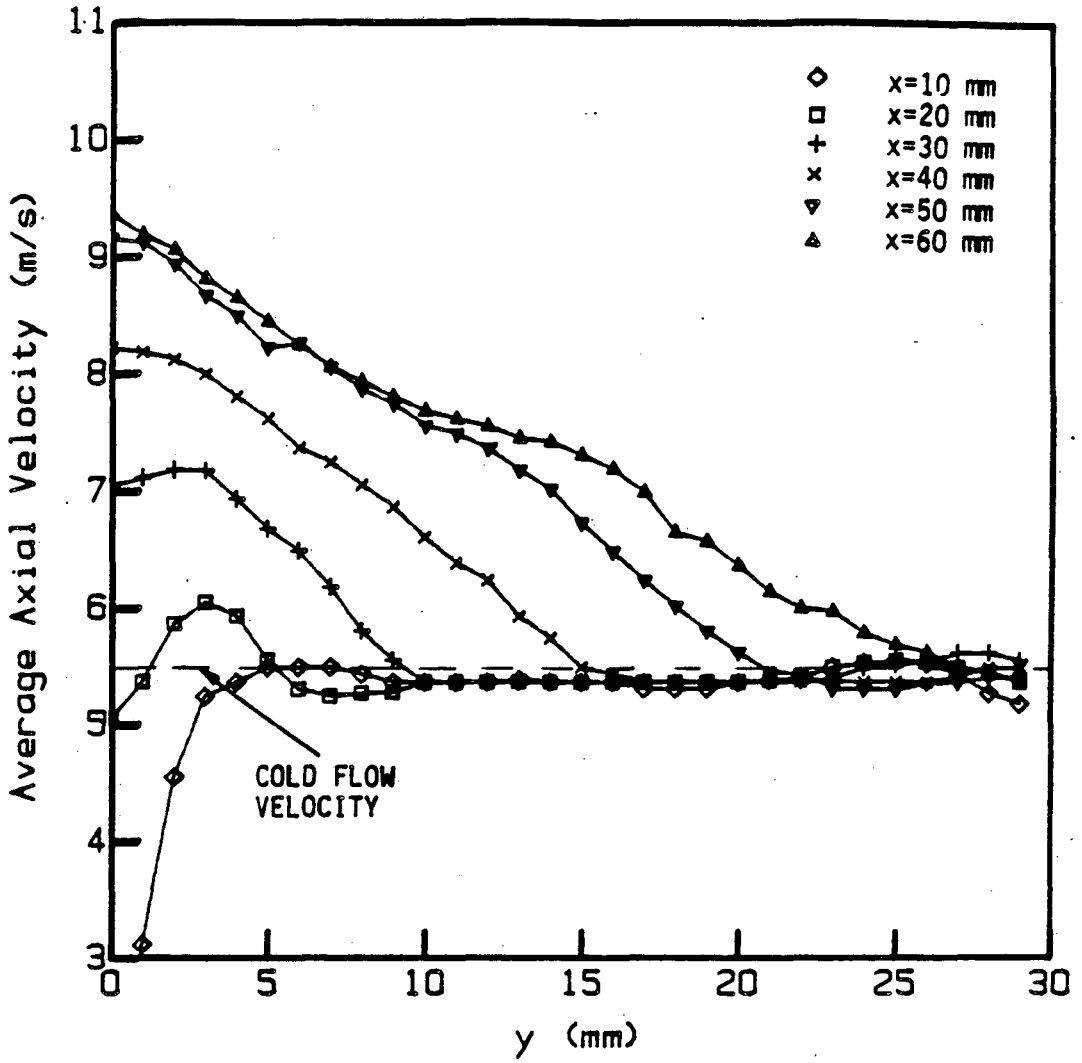
x=10 mm
x=20 mm
x=30 mm
x=40 mm
x=50 mm
x=60 mm
COLD FLOW
VELOCITY
Average Axial Velocity (m/s)
y (mm)
11
10
9
8
7
6
5
4
3
0
5
10
15
20
25
30

Figure 10

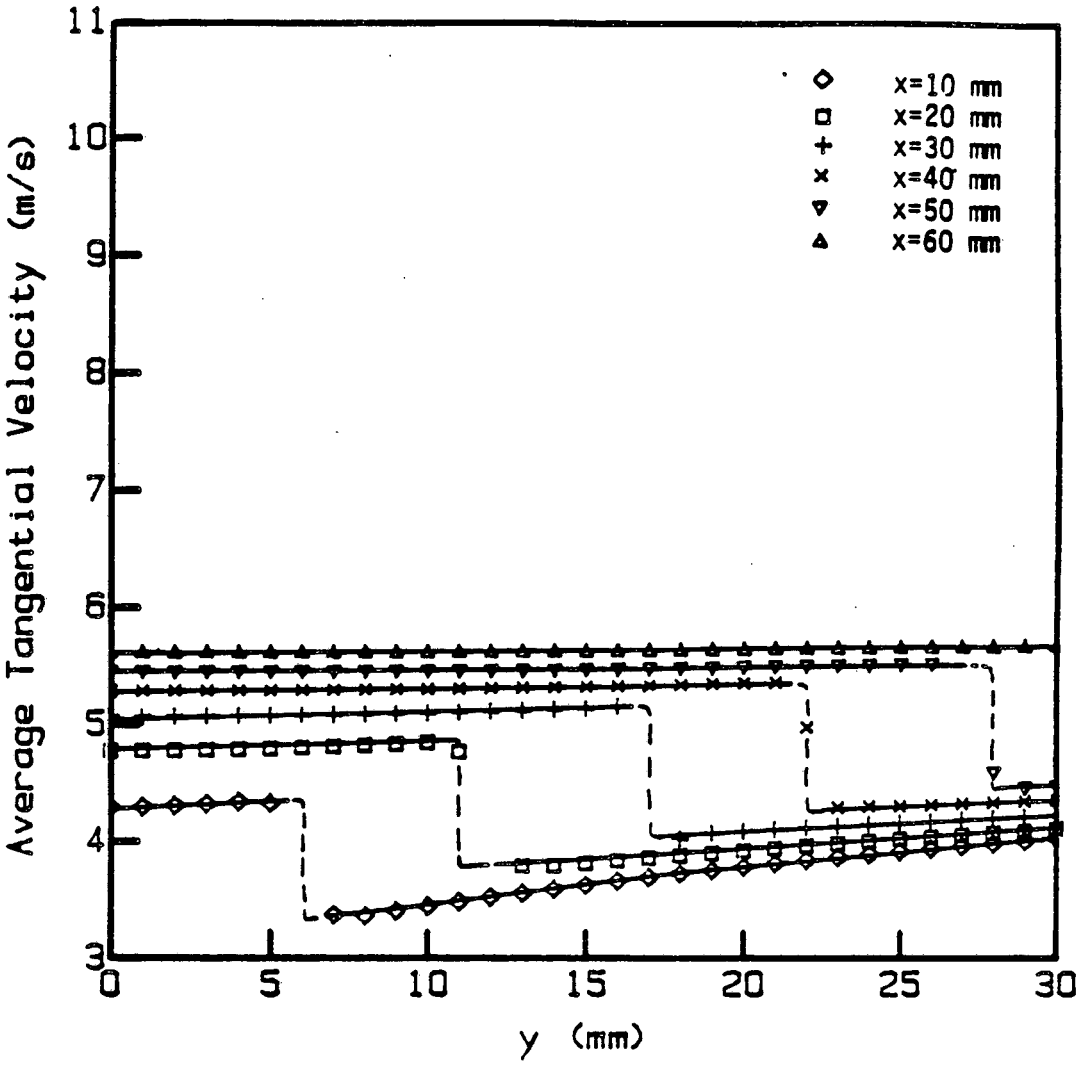
Average Tangential Velocity (m/s)
y (mm)
x=10 mm
x=20 mm
x=30 mm
x=40 mm
x=50 mm
x=60 mm
11
10
9
8
7
6
5
4
3
0
5
10
15
20
25
30

Figure 11

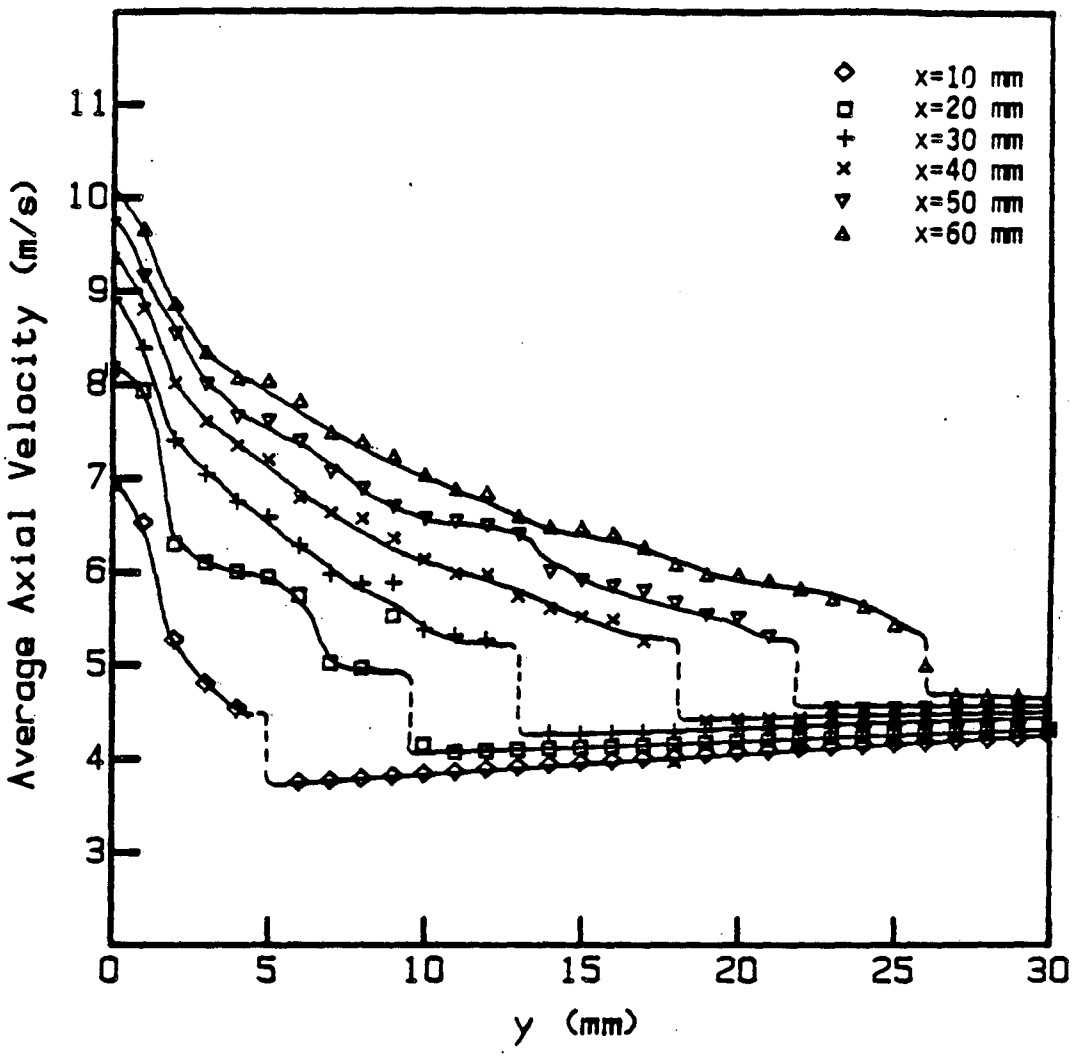
x=10 mm
x=20 mm
x=30 mm
x=40 mm
x=50 mm
x=60 mm
Average Axial Velocity (m/s)
11
10
9
8
7
6
5
4
3
0
5
10
15
20
25
30
y (mm)

Figure 12

This report was done with support from the Department of Energy. Any conclusions or opinions expressed in this report represent solely those of the author(s) and not necessarily those of The Regents of the University of California, the Lawrence Berkeley Laboratory or the Department of Energy.

Reference to a company or product name does not imply approval or recommendation of the product by the University of California or the U.S. Department of Energy to the exclusion of others that may be suitable.

LAWRENCE BERKELEY LABORATORY
TECHNICAL INFORMATION DEPARTMENT
UNIVERSITY OF CALIFORNIA
BERKELEY, CALIFORNIA 94720